Calhoun
Institutional Archive of the Naval Postgraduate School

Calhoun: The NPS Institutional Archive

DSpace Repository

Faculty and Researchers | Faculty and Researchers' Publications

2014

Sources of nitrate in stratocumulus cloud water: Airborne measurements during the 2011 E-PEACE and 2013 NiCE studies

Prabhakar, Gouri; Ervens, B.; Wang, Z.; Maudlin, L.C.; Coggon, M.M.; Jonsson, H.H.; Seinfeld, J.H.; Sorooshian, A.

Elsevier Ltd.

Prabhakar, Gouri, et al. "Sources of nitrate in stratocumulus cloud water: Airborne measurements during the 2011 E-PEACE and 2013 NiCE studies." Atmospheric Environment 97 (2014): 166-173.
https://hdl.handle.net/10945/49708

This publication is a work of the U.S. Government as defined in Title 17, United States Code, Section 101. Copyright protection is not available for this work in the

Downloaded from NPS Archive: Calhoun

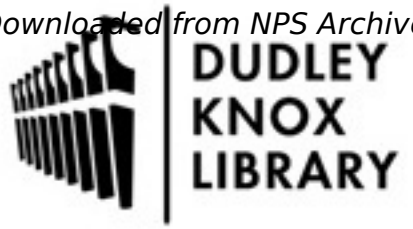

http://www.nps.edu/library

Calhoun is the Naval Postgraduate School's public access digital repository for research materials and institutional publications created by the NPS community. Calhoun is named for Professor of Mathematics Guy K. Calhoun, NPS's first appointed -- and published -- scholarly author.

Dudley Knox Library / Naval Postgraduate School
411 Dyer Road / 1 University Circle
Monterey, California USA 93943

Atmospheric Environment 97 (2014) 166–173

Contents lists available at ScienceDirect

Atmospheric Environment

journal homepage: www.elsevier.com/locate/atmosenv

Sources of nitrate in stratocumulus cloud water: Airborne measurements during the 2011 E-PEACE and 2013 NiCE studies

Gouri Prabhakar [a], B. Ervens [b, c], Z. Wang [d], L.C. Maudlin [a], M.M. Coggon [e], H.H. Jonsson [f], J.H. Seinfeld [e], A. Sorooshian [a, d, *]

[a] Department of Atmospheric Sciences, University of Arizona, Tucson, AZ, USA
[b] CIRES, University of Colorado, Boulder, CO, USA
[c] NOAA, ESRL/CSD Boulder, CO, USA
[d] Department of Chemical and Environmental Engineering, University of Arizona, Tucson, AZ, USA
[e] Department of Chemical Engineering, California Institute of Technology, Pasadena, CA, USA
[f] Naval Postgraduate School, Monterey, CA, USA

HIGHLIGHTS

- The major sources of NO_3^- in the study region are ship and fire emissions.
- Entrainment of wildfire emissions can significantly increase NO_3^- in clouds.
- Nitrate is associated with crustal particles in the coastal region.
- The nitrate-to-sulfate mass ratio decreases rapidly with cloud height.
- Volatilization during drop evaporation pushes NO_3^- to the gas phase.

GRAPHICAL ABSTRACT

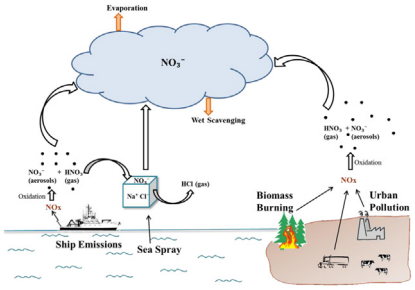

ARTICLE INFO

Article history:
Received 18 March 2014
Received in revised form
6 August 2014
Accepted 8 August 2014
Available online 9 August 2014

Keywords:
Cloud water
Chloride depletion
Stratocumulus
Marine
Biomass burning
Sea-salt

ABSTRACT

This study examines the sources of NO_3^- in stratocumulus clouds over the eastern Pacific Ocean off the California coast using airborne and surface measurement data from the Eastern Pacific Emitted Aerosol Cloud Experiment (E-PEACE; 2011) and Nucleation in California Experiment (NiCE; 2013). Average NO_3^- air-equivalent concentrations in cloud water samples categorized as having been influenced by ship exhaust (2.5 μg m^{-3}), strong marine emissions (2.5 μg m^{-3}) and fires (2.0 μg m^{-3}) were more than twice that in the background cloud water (0.9 μg m^{-3}). During periods when biomass burning plumes resided above cloud top, 16 of 29 cloud water samples were impacted due to instability in the entrainment interface layer with NO_3^- levels reaching as high as 9.0 μg m^{-3}. Nucleation scavenging of chloride depleted sea-salt is a source of cloud water NO_3^-, with the lowest Cl^-:Na^+ ratio (1.5) observed in ship-influenced samples. Surface aerosol measurements show that NO_3^- concentrations peak in the particle diameter range of 1.0–5.6 μm, similar to Na, Cl^- and Si, suggesting that drop activation of crustal particles and sea salt could be an important source of NO_3^- in cloud water. The contrasting behavior of NO_3^- and SO_4^{2-} is emphasized by the NO_3^-:SO_4^{2-} mass concentration ratio which is highest in cloud water (by more than a factor of two) followed by above cloud aerosol, droplet residual particles, and below cloud aerosol. Trends of a decreasing NO_3^-:SO_4^{2-} ratio with altitude in clouds are confirmed by parcel model studies due to the higher rate of in-cloud sulfate formation as compared to HNO_3 uptake by droplets.
© 2014 Elsevier Ltd. All rights reserved.

* Corresponding author. PO Box 210011, Tucson, AZ 85721, USA.
E-mail address: armin@email.arizona.edu (A. Sorooshian).

http://dx.doi.org/10.1016/j.atmosenv.2014.08.019
1352-2310/© 2014 Elsevier Ltd. All rights reserved.

1. Introduction

Nitrate (NO_3^-) is a key inorganic anion in cloud water that can alter microphysical properties in clouds, influence aqueous-phase processes in drops and affect ecosystems after wet deposition. The uptake of nitric acid (HNO_3) by aerosol particles enhances their cloud drop nucleating ability and can lead to increases in both cloud drop number concentration and cloud albedo (Xue and Feingold, 2004; Makkonen et al., 2012); uptake of HNO_3 by cloud drops can also increase the hygroscopicity of cloud droplet residual particles after drop evaporation (Henning et al., 2014). Negative radiative forcing from nitrate-containing particles has been projected by global aerosol models to increase due to future elevated levels of nitrate precursors (Liao et al., 2006; Bauer et al., 2007). It is important to understand the factors governing nitrate concentrations in marine clouds.

The goal of this study is to use airborne chemical measurements off the California coast to identify sources of NO_3^- in marine cloud water and factors that dictate the strength of their influence on NO_3^- concentrations. Airborne measurements from two flight campaigns, NiCE and E-PEACE, have been utilized to evaluate processes through which NO_3^- enters cloud water (nucleation scavenging and uptake of gas-phase HNO_3). The persistent summertime stratocumulus cloud deck in the study region provides a tailor-made venue for this type of investigation, as it is impacted by a number of different sources enriched with NO_3^- precursors such as ships, wildfires, and continental anthropogenic emissions. This study benefits from the rapid sampling of cloud water to provide a high level of spatiotemporal resolution, especially vertically in clouds.

2. Experimental methods

2.1. Flight campaign descriptions

2.1.1. Nucleation in California Experiment (NiCE), 2013

The Center for Interdisciplinary Remotely – Piloted Aircraft Studies (CIRPAS) Twin Otter conducted 23 flights during the Nucleation in California Experiment (NiCE) between July and August in 2013 over the Pacific Ocean off the central California coast (34°N–43°N, 119°W–126°W). Two major aims of NiCE were to study (i) the dependence of cloud properties on environmental conditions, and (ii) nucleation events from urban pollution, animal husbandry and biogenic emissions. During NiCE, a number of wildfires occurred near the California–Oregon border, smoke from which was transported to the study region with the potential to impact clouds.

2.1.2. Eastern Pacific Emitted Aerosol Cloud Experiment (E-PEACE), 2011

Thirty research flights were conducted with the Twin Otter during the Eastern Pacific Emitted Aerosol Cloud Experiment (E-PEACE), conducted between July and August in 2011, to study aerosol–cloud–precipitation–radiation interactions in the same region as NiCE with a nearly identical instrument payload. A general overview of the E-PEACE campaign is provided by Russell et al. (2013). The present study is primarily based on measurements made during NiCE; however, data from E-PEACE are included to provide additional statistics and thus more confidence for a subset of the results.

2.2. Airborne measurements

Twin Otter measurements focused on microphysical properties of particles and clouds in addition to meteorological variables. Nearly all flights consisted of level legs below cloud, in cloud (cloud base, mid-cloud, cloud top) and above cloud. Cloud water was collected using a modified Mohnen slotted-rod cloud water collector (Hegg and Hobbs, 1986). These samples were collected over a 10–30 min duration in high-density polyethylene bottles. The collector was inserted upwards through a port at the top of the aircraft during cloud passes. A total of 119 and 87 samples were collected in NiCE and E-PEACE, respectively. The collection efficiency of the collector is inversely related to the speed of the aircraft with little correlation with drop mass mean diameter up to ~35 μm (Hegg and Hobbs, 1986). Samples were tested for pH (Oakton Model 110 pH meter calibrated with pH 4.01 and pH 7.00 buffer solutions) and treated with 5 μL chloroform to prevent subsequent biological processing. Detailed analysis of chemical composition was conducted with ion chromatography (IC; Thermo Scientific Dionex ICS – 2100 system) and inductively coupled plasma mass spectrometry (ICP-MS; Agilent 7700 Series). Tables S1–S2 (Supplement) report limits of detection, precision, and cloud water blank sample concentrations for species measured by the IC. The charge balance of ionic species measured by the IC in cloud water samples exhibits a best-fit slope (positive charges on *y*-axis) of 1.02 ± 0.01 (Fig. S1 in Supplement). Elemental concentrations reported by the ICP-MS are the averages over three measurements, with standard deviations less than 3%. The limits of detection of all species were in the ppt level. More details about these techniques are provided elsewhere (Sorooshian et al., 2013; Wang et al., 2014).

Sub-micrometer non-refractory aerosol composition measurements were conducted with a compact time-of-flight aerosol mass spectrometer (C-ToF-AMS, Aerodyne) (Drewnick et al., 2005). In clear air, particles were sampled through a sub-isokinetic aerosol inlet (Hegg et al., 2005). When in clouds, the C-ToF-AMS sampled cloud drop residual particles downstream of a counterflow virtual impactor (CVI). The efficiency of drop entry into the CVI increases with drop size with a $D_{p,50}$ of 11 μm, but there is decreasing transmission efficiency with increasing drop size inside the inlet mainly owing to inertial deposition (Shingler et al., 2012). Shingler et al. (2012) reported that the $D_{p,50}$ of the CVI was sufficiently low to sample the majority of the drop distribution during flights in the study region with the exception of periods near cloud bases, especially when influenced by ship plumes. Droplet number concentration, N_d (cm^{-3}), was measured by a cloud aerosol spectrometer (CAS), and liquid water content (LWC) was obtained with a PVM-100 probe (Gerber et al., 1994). Sub-cloud particle number concentrations in the diameter ranges 0.01–1.0 μm and 0.1–2.6 μm were obtained using a condensation particle counter (CPC 3010; TSI Inc.) and a passive cavity aerosol spectrometer probe (PCASP), respectively.

While the NO_3^- fraction of sea salt is negligible, the non-sea salt (NSS) fraction of SO_4^{2-} in cloud water is calculated using Na^+ concentrations (SO_4^{2-}:Na^+ is ~0.25 by weight for sea salt; Seinfeld and Pandis, 2006). Henceforth, SO_4^{2-} refers to NSS SO_4^{2-}. Liquid-phase concentrations of cloud water species were converted to air-equivalent concentrations by multiplication with the average LWC measured during the cloud water collection time. A threshold LWC value of 0.02 g m^{-3} is used to define periods in clouds.

2.3. Ground measurements

Size-resolved aerosol composition measurements were conducted during NiCE ~4 km from the coast in Marina, CA with a 10-stage micro-orifice uniform deposit impactor (MOUDI; M110-R, MSP Corporation; Marple et al., 1991). The 50% cut-off sizes of the MOUDI, assuming flat impaction surfaces, are 0.056, 0.1, 0.18, 0.32, 0.56, 1.0, 1.8, 3.2, 5.6, 10 and 18 μm in aerodynamic diameter. The

cut sizes for the Teflon filters (PTFE membrane, 2 μm pore, 46.2 mm, Whatman) may be slightly modified depending on their surface roughness (Marjamaki and Keskinen, 2004; Fujitani et al., 2006). The samples were collected over a duration of 96 h with a flow rate of 30 L min^{-1}. The filters were cut in half and only one half was extracted for chemical characterization of the samples. Extractions were performed by using 10 mL of milli-Q water in sealed glass vials that were sonicated at 30 °C for 20 min. Extracts were refrigerated prior to being analyzed with ICP-MS and IC. MOUDI species examined here include NO_3^-, SO_4^{2-}, Cl^-, Na and Si, where concentrations of only the latter two are from ICP-MS.

3. Results and discussion

3.1. Major emissions sources (NiCE data)

Nitrate was the fourth most abundant water-soluble species in cloud water during NiCE, after Na^+, Cl^- and SO_4^{2-}. Average NO_3^- air-equivalent concentrations in the study region (1.5 ± 1.6 μg m^{-3}) are similar in magnitude to those measured in North Atlantic marine clouds influenced by continental European air masses (2.1 ± 1.2 μg m^{-3}; Borys et al., 1998), the southeast Pacific Ocean (~0.7 μg m^{-3}; Benedict et al., 2012) and off the southern California coast (~0.6 μg m^{-3}; Straub et al., 2007).

NiCE cloud water data are further grouped into four major categories ("ship", "fire", "low Cl^- marine" and "high Cl^- marine") for a quantitative comparison between the different sources (Table 1). Cloud water samples with sub-cloud (immediately below cloud base) maximum CPC concentrations >900 cm^{-3} and vanadium (V) >1 ng m^{-3} are classified in the ship category; measurements in the region have identified V as a ship exhaust tracer (Coggon et al., 2012). In addition to visual and olfactory evidence, samples with above-cloud maximum PCASP concentrations >1000 cm^{-3} are considered in the fire category; biomass burning plumes during NiCE produced particles with diameters predominantly above 100 nm, which is the lower size limit of the PCASP. Despite the presence of smoke above the clouds, not all cloud water samples shared evidence of smoke, as discussed in Section 3.2.3. Hence, the fire group was divided further into two sub-groups: samples with and without smoke entrainment. The remainder of the samples were influenced predominantly by marine emissions; those exhibiting Cl^- concentrations exceeding 11 μg m^{-3} (i.e. average measured during NiCE) were identified as "high Cl^- marine" while the rest were categorized as "low Cl^- marine". These latter samples do not necessarily represent pristine conditions since the majority of the study region is influenced by aged anthropogenic emissions, mainly from ships (Coggon et al., 2012). While not a specifically designated category, continental emissions (biogenic and anthropogenic) other than from fires can also influence the regional clouds (Coggon et al., 2014). Air-equivalent NO_3^- concentrations in cloud water samples characterized as "high Cl^- marine" (2.5 ± 1.9 μg m^{-3}), "ship" (2.5 ± 2.1 μg m^{-3}) and "fire" with entrainment (2.0 ± 2.2 μg m^{-3}) are more than twice those than in "low Cl^- marine" category (0.9 ± 0.7 μg m^{-3}). Nitrate in samples with smoke entrainment reached values as high as 9.0 μg m^{-3}; however, fire samples not characterized by smoke entrainment exhibited comparable NO_3^- levels to "low Cl^- marine" samples.

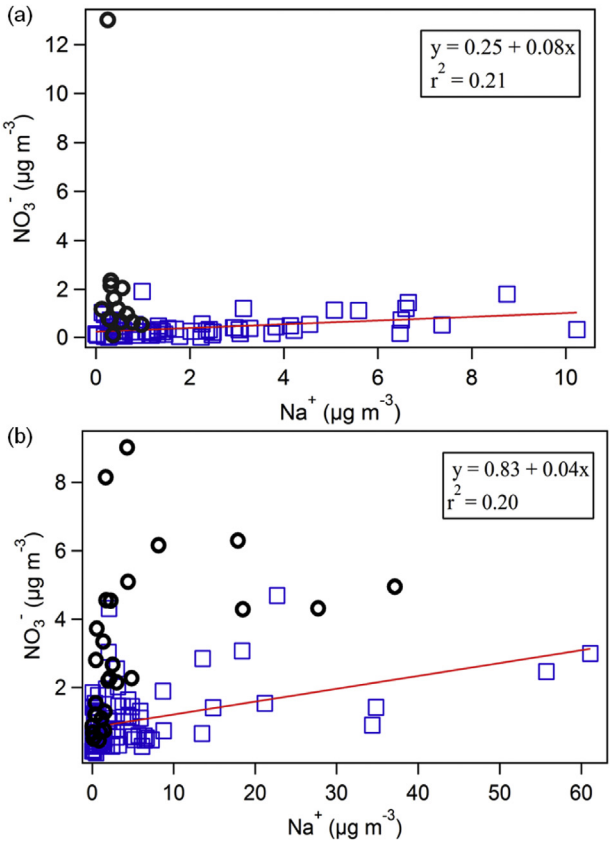

Fig. 1. Plot of cloud water NO_3^- versus cloud water Na^+ measured during (a) E-PEACE and (b) NiCE. The square markers are samples with low vanadium, V (<1 ng m^{-3}). The circular markers are samples with higher V (>1 ng m^{-3}). The straight lines and insert equations are associated with the linear fits (significant at the 95% confidence level) between NO_3^- and Na^+ for low V conditions. All species in cloud water are reported in air-equivalent concentrations.

Table 1 also reports chemical mass concentration ratios intended to further support the sample grouping criteria, as each emission source is characterized by specific tracer species that are used in the ratios. Oxalate and NSS K^+ are commonly used as chemical tracers for biomass burning emissions. However, NSS K^+ exhibited highest concentrations in ship influenced samples, whereas oxalate was highest in fire samples and thus chosen as the fire tracer. Ratios of [Oxalate]:[Na^+] and [Oxalate]:[V] are used to

Table 1
Summary of the average chemical characteristics of NiCE cloud water samples categorized based on the emissions source they are most strongly influenced by. Concentrations are reported in air-equivalent units (μg m^{-3}). Sample number is shown in parentheses.

	High Cl^- marine	Ship	Fire (with smoke entrainment)	Fire (no smoke entrainment)	Low Cl^- marine
Nitrate (μg m^{-3})	2.5 ± 1.9 (12)	2.5 ± 2.1 (17)	2.0 ± 2.2 (16)	0.6 ± 0.4 (13)	0.9 ± 0.7 (49)
	max = 6.2	max = 8.2	max = 9.0	max = 1.3	max = 3.7
Oxalate (μg m^{-3})	0.2 ± 0.2 (12)	0.2 ± 0.2 (17)	0.5 ± 0.6 (16)	0.11 ± 0.07 (13)	0.10 ± 0.07 (49)
	max = 0.5	max = 0.7	max = 2.7	max = 0.3	max = 0.4
pH	4.2 ± 4.3 (11)	4.1 ± 4.3 (15)	4.1 ± 4.2 (15)	4.3 ± 4.8 (12)	4.3 ± 4.5 (48)
Cl^-:Na^+	1.8 ± 0.1 (11)	1.5 ± 0.3 (17)	1.7 ± 0.2 (16)	1.7 ± 0.1 (13)	1.8 ± 1.1 (49)
Oxalate:Na^+	0.01 ± 0.02 (11)	0.3 ± 0.3 (17)	0.4 ± 0.4 (16)	0.3 ± 0.5 (13)	0.2 ± 0.2 (49)
Oxalate:V	202 ± 68 (10)	100 ± 135 (16)	725 ± 437 (15)	387 ± 297 (13)	178 ± 105 (45)

distinguish fire samples from "high Cl^- marine" (high Na^+) and ship samples (high V), respectively. Average values of both ratios are the highest in fire influenced samples, while [Oxalate]:[Na^+] and [Oxalate]:[V] are lowest in the "high Cl^- marine" and ship categories, respectively. Therefore, the ratio results show that the categorization criteria are suitable to distinguish between samples clearly influenced by either fires, ships, or strong marine emissions. It is worth noting that the most acidic samples were in the ship (pH = 4.1) and fire influenced (pH = 4.1) categories (Table 1).

3.2. Pathways of nitrate into and out of cloud water

3.2.1. Nucleation scavenging and chloride depletion

Nitrate can enter cloud drops through drop activation of NO_3^--containing particles. Nitric acid is known to replace Cl^- in sea salt (NaCl) to form $NaNO_3$ and release gaseous HCl (Seinfeld and Pandis, 2006). The average mass ratio of Cl^-:Na^+ was lower than the ideal value of 1.8 (composition of natural sea salt; Seinfeld and Pandis, 2006) in all categories except "low/high Cl^- marine" (Table 1). This is suspected to be a result of chloride depletion by strong acids like HNO_3 and H_2SO_4. The ratio was the lowest (1.5) in the ship category due to substantial NO_x emissions and low ammonia concentrations resulting in higher amounts of HNO_3. Cloud water NO_3^- increased as a function of cloud water sodium (Na^+) under low ship influence (indicated by V) during both campaigns (Fig. 1). In cases of direct ship emissions (V > 1 ng m^{-3}), NO_3^- concentrations in cloud water were much higher due to the likely dissolution of HNO_3. The linear relationship between NO_3^- and Na^+ is supportive of chloride-depleted sea salt being a potential pathway for cloud water NO_3^- via nucleation scavenging, assuming the source of Na^+ in cloud water is sea salt. Crustal dust naturally contains Na^+, which is ~1.9% of Si by mass (Seinfeld and Pandis, 2006); even if the highest Si air-equivalent concentration measured in cloud water during NiCE (0.44 μg m^{-3}) is assumed to be from continental wind-blown dust, the contribution of dust to cloud water Na^+ would be less than 1% of the total Na^+ measured in the cloud water samples. It is noted here that some of the displaced HCl may be scavenged by cloud droplets before removal by dry or wet deposition to the sea surface.

The cloud water data suggest that nitric acid partitions to sea salt and crustal particles, which can activate into drops, and the NiCE MOUDI data allow for confirmation that NO_3^- is contained in such particles. The mass concentrations of NO_3^-, Na, Cl^- and Si peak between 1.0 and 5.6 μm (Fig. 2). Elemental Na mass concentrations measured by ICP-MS are used here (instead of Na^+) to include all sources of Na. Fig. 2 suggests that NO_3^- is associated with sea salt and Si-enriched particles. While Na and Cl^- are the major components of sea salt, Si and Na are components of crustal dust in addition to various other sources such as fly ash, ship emissions, and biomass burning (Furutani et al., 2011). The role of these coarse particles as a sink for HNO_3 is especially important when ammonium nitrate formation is not favored such as in the study region, which is characterized by slight acidity (Table 1).

3.2.2. Nitrate:sulfate ratio in and around clouds

The concentration ratio of NO_3^- to SO_4^{2-} offers insights into the extent to which partitioning to cloud drops is more important relative to nucleation scavenging of cloud condensation nuclei (CCN) containing these species. For instance, one airborne-based study in the vicinity of Ohio indicated that NO_3^- enters cloud water predominantly through partitioning of gaseous HNO_3, whereas SO_4^{2-} enters mostly through nucleation scavenging (Hayden et al., 2008). That study found the highest NO_3^-:SO_4^{2-} ratios in bulk cloud water, followed by cloud droplet residual particles and sub-cloud particles. Drewnick et al. (2007) separately showed that for Mt. Åreskutan in central Sweden the NO_3^- fraction in droplet residual particles was much larger than in ambient particles in contrast to SO_4^{2-}, which exhibited a higher mass fraction in ambient particles. They suggested that particles predominantly comprised of NO_3^- were more efficiently activated to form cloud drops relative to those enriched with SO_4^{2-}; furthermore, they concluded that scavenging of vapors (e.g., HNO_3) by drops was not responsible for their results. Different conclusions in these two studies motivate an analysis of how this chemical mass concentration ratio varies inside and outside of clouds in our study region.

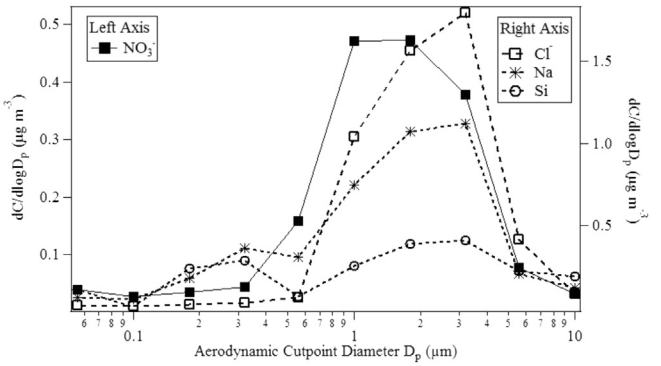

Fig. 2. Speciated aerosol mass size distributions measured at a coastal ground site in the study region during the NiCE campaign.

During E-PEACE and NiCE, the highest values of NO_3^-:SO_4^{2-} were measured in cloud water as compared to C-ToF-AMS measurements outside of cloud and downstream of the CVI in cloud (Fig. 3). It is noted that C-ToF-AMS NO_3^- generally was below detection limits on cloud-free days in the marine boundary layer. The peak ratio in cloud water could be a result of (i) an increase in cloud water NO_3^- through uptake of HNO_3, or (ii) NO_3^- in coarse and/or refractory particles that served as CCN not measured by the C-ToF-AMS. The average NO_3^-:SO_4^{2-} ratio in cloud water was higher during NiCE (2.45 ± 2.8) as compared to E-PEACE (0.4 ± 1.1) due largely to higher NO_3^- concentrations from biomass burning that occurred only during NiCE. Sulfate concentrations were more comparable in both experiments (0.78 and 1.12 μg m^{-3} in NiCE and E-PEACE, respectively). The NO_3^-:SO_4^{2-} ratio above cloud tops was consistently higher than that below clouds (4.3 times higher for both campaigns combined) due to more sub-cloud SO_4^{2-} from stronger sources such as ships and dimethylsulfide, and enhanced NO_3^- from biomass burning residing above cloud top in the case of NiCE. Average C-ToF-AMS NO_3^- (SO_4^{2-}) levels above and below cloud were 0.40 (0.69) and 0.14 (0.92) μg m^{-3} for NiCE, respectively, and 0.04 (0.42) and 0.05 (1.23) for E-PEACE. Although higher than the sub-cloud average value, the NO_3^-:SO_4^{2-} ratio in cloud droplet residual particles was considerably lower than that in cloud water (80% lower during E-PEACE and 79% lower during NiCE). This is most likely the result of volatization of NO_3^-, unlike SO_4^{2-}(Hayden et al., 2008); the heated air stream in the CVI inlet ranged between approximately 30–35 °C.

3.2.3. Case studies of biomass burning influence on cloud water nitrate

Flight 16 measurements during NiCE (N16), conducted on 29 July 2013, were influenced by smoke from the Big Windy and Whiskey Complex forest fires in southwest Oregon. Biomass burning releases NO_x that is photochemically oxidized to HNO_3, which could then be neutralized by alkaline species. Nitric acid can partition to particles, such as those in the coarse size range (Fig. 2), and be transported over long distances (Ruellan et al., 1999). The concentration of super-100 nm particles in the free troposphere

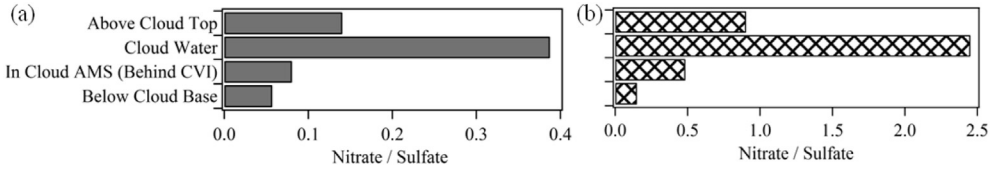

Fig. 3. Average values of the NO_3^-:SO_4^{2-} mass concentration ratio below, in and above cloud during (a) E-PEACE and (b) NiCE.

was enhanced (maximum concentration = 4608 cm^{-3}) due to wildfire smoke (Fig. 4a). Although cloudy areas sampled during the flight had a thick layer of smoke above them, the cloud water samples were not influenced by the smoke to the same extent. Three cloud water samples (#90, #96 and #97), roughly within ~30–50 km of each another, are discussed to illustrate this point. Samples 96 and 97 (unlike Sample 90) exhibited significantly higher concentrations of NO_3^-, K, Ca, Mn, Al, Cl^- and oxalate (Fig. 5). These species have been measured in emissions from biomass burning in other regions (Hays et al., 2002; Wonaschütz et al., 2011). The higher concentrations of Al and Ca in Samples 96 and 97 relative to Sample 90 are also consistent with the lofting of soil dust during wildfires (Clements et al., 2008; Kavouras et al., 2012).

The smoke above clouds must be entrained into the clouds in order to alter cloud properties. Entrainment of the biomass burning plume in Samples 96 and 97 resulted in an increase in number concentration of super-100 nm particles below cloud top (Fig. 4a). Entrainment of free tropospheric air into clouds is governed by the stability of flow in a narrow layer immediately above the cloud top, called the entrainment interface layer (EIL). The EIL is treated here as a ~20 m thick layer above the cloud tops (Haman et al., 2007). Enhanced turbulent flow in the EIL promotes more entrainment of free tropospheric air into the clouds. Atmospheric turbulence is quantified by the gradient Richardson Number, *Ri*, which accounts for both static and mechanical instabilities:

$$Ri = \frac{g}{\overline{\theta_v}} \frac{\partial\theta_v/\partial z}{\left(\partial u/\partial z\right)^2 + \left(\partial v/\partial z\right)^2} \quad (1)$$

where g is acceleration due to gravity (9.8 m s^{-2}), θ_v is the virtual potential temperature (K), u and v are components of the horizontal wind (m s^{-1}) in the EIL, and z is the thickness of the EIL (~20 m from cloud top). When applied to a layer of finite thickness, this is called the bulk gradient Richardson Number, Ri_b. If $Ri_b < 0$, the layer is statically (or thermally) unstable and leads to convection within the layer. If $Ri_b > 0$, the layer is statically stable but if it gets lower than the critical value (R_c) of 0.25, non-turbulent flow will become turbulent due to mechanical instability. Once Ri_b becomes greater than the termination value (R_T) of 1, the flow will become non-turbulent (Stull, 2003). For Sample 90, which was collected between 10:43 and 10:53 (Local Time, LT), the EIL was non-turbulent (Ri_b is 1.7). In contrast, Samples 96 and 97, which were collected later in the day (13:08–13:15 and 13:29–13:43 LT, respectively), were obtained in the presence of high shear in horizontal winds in the EIL. The Ri_b value for Samples 96 and 97 was 0.29 and 0.21, respectively, and thus the EIL above these two samples was turbulent (Fig. 4b), resulting in entrainment of the free tropospheric smoke into the cloud. It must be noted here that there is a hysteresis effect in the behavior of turbulent flow because $R_c < R_T$. Hence, relevant to the

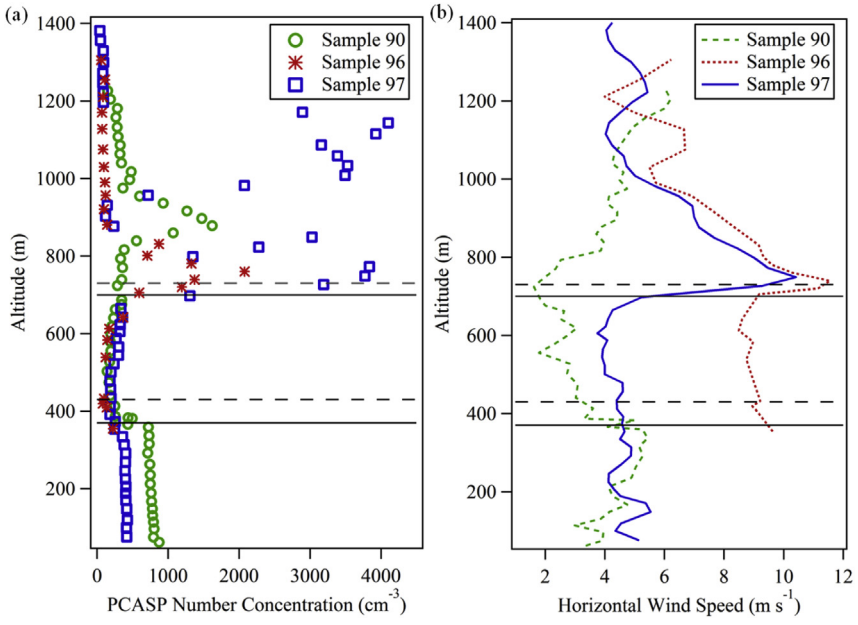

Fig. 4. Vertical profiles of (a) number concentration of super-100 nm particles (from PCASP) and (b) horizontal wind speed for three cloud water samples collected during NiCE. Samples 96 and 97 experienced entrainment of smoke at cloud top unlike Sample 90. The solid horizontal lines represent the cloud base and top for Sample 96. The dashed lines represent the cloud base and top for Samples 90 and 97.

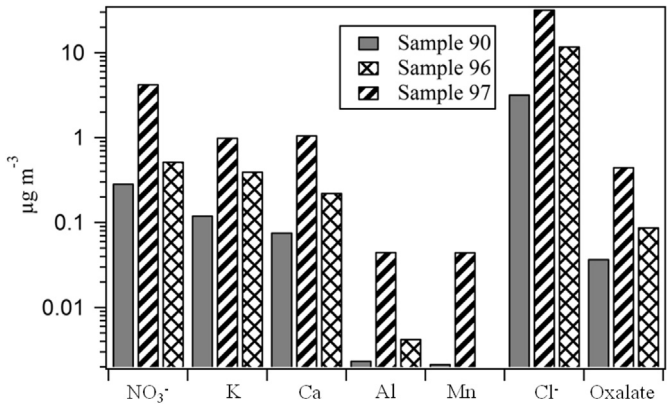

Fig. 5. Chemical composition (air-equivalent units) of three cloud water samples from NiCE Research Flight 16 conducted on 29 July 2013 with varying influence from biomass burning plumes above cloud top.

categorization in Table 1, for samples with Ri_b values between 0.25 and 1, and samples with missing meteorological measurements, the vertical distributions of PCASP number concentration were used to identify turbulence and thus entrainment.

3.3. Vertical profiles of the nitrate:sulfate ratio in clouds

3.3.1. Model set-up

To explore processes affecting the relative concentration of nitrate and sulfate in clouds, a parcel model is used to simulate the ascent of an air parcel along a trajectory of a typical stratocumulus cloud, as derived from large eddy simulations (Ervens et al., 2004). The model is initialized with aerosol size distributions (~20 < D_p < ~900 nm) that represent the encountered source characteristics (Table S3). These particles are activated into cloud droplets according to Köhler theory, near cloud base when the air is supersaturated with respect to water vapor. At each model time step, the trajectory prescribes temperature, pressure, and total water mixing ratio in the ascending air parcel. The simulations start just below cloud base (RH ~ 99%). Below a threshold of LWC of 0.01 g m^{-3}, only chemical processes in the gas phase are considered which include the oxidation of volatile organic compounds and NO_x by OH and O_3; above this limit, uptake of soluble gases and their processing in the aqueous phase are simulated. Initial conditions for "low Cl^- marine", "ship" and "fire", as encountered during NiCE, are summarized in Table S3 (Supplement). The resulting drop size distribution is treated explicitly, and the chemical composition of each drop size class is a result of the dissolution of the initial CCN (ammonium, sulfate, nitrate), the trace gases that are taken up (e.g., HNO_3, SO_2) and the chemical reactions in each droplet (i.e. sulfate formation as a function of S(IV), H_2O_2 and H^+ concentration). To be noted here is that the drop size spectrum changes over the course of the simulation since droplets grow during their ascent in a cloud. The drop size distributions for all three cases near cloud base, in the middle of the cloud and at cloud top are shown in Fig. S2 (Supplement), together with the averaged measured drop size distribution. The initial aerosol population is tracked on a moving mass grid where mass addition occurs due to HNO_3 uptake and formation of sulfate mass upon S(IV) oxidation in the aqueous phase by H_2O_2 and ozone. We do not include SO_2 oxidation by OH radicals in the gas phase since it has been shown that in the presence of clouds the conversion of S(IV) into sulfate in the aqueous phase by H_2O_2 and O_3 is much more efficient than in the gas phase (e.g., Cautenet and Lefeivre, 1994).

3.3.2. Comparison of observed and predicted nitrate:sulfate ratios

Fig. 6 compares the observed (from NiCE) and predicted NO_3^-:SO_4^{2-} ratios for the three cases as a function of cloud normalized height (0 = base, 1 = top); individual SO_4^{2-} and NO_3^- concentrations are reported in Fig. S3a, while HNO_3 levels (with and without uptake by drops) are shown in Fig. S3b. The simulated cloud thickness was ~200 m, which is similar to the average thickness of clouds during NiCE. Fig. 6a shows a decrease in the NO_3^-:SO_4^{2-} ratio with height due to rapid oxidation of S(IV) in cloud water. Once this precursor is consumed, the ratio is predicted to increase a little due to continuous NO_x oxidation and is mostly caused by HNO_3 uptake into cloud water. The majority of HNO_3 is scavenged by the cloud droplets, mostly near cloud base (Fig. S3b). The formation of sulfate occurs on longer time scales (Fig. S3a), which can be explained by the multistep pathway (i.e. uptake of SO_2 and oxidants and subsequent aqueous reaction) as opposed to the direct uptake of HNO_3.

As compared to the other two conditions, measurements of the NO_3^-:SO_4^{2-} ratio for the fire (with entrainment) category exhibited a larger deviation from the predicted ratio in the top half of clouds. This can be explained by the enhanced turbulent cloud structure leading to entrainment of biomass burning plumes from cloud top. The parcel model assumes that air including all precursor gases is transported upwards from cloud base and does not take into account any additional entrainment processes for trace gases other than water vapor. For such convective cases, the spatial trend of NO_3^-:SO_4^{2-} can be equated to its temporal evolution and can be used as a measure of aerosol processing due to multiphase processes. This assumption might be valid for cloud evolution in marine air and ship plumes but fails if turbulent processes lead to mixing of both (processed) aerosol particles and trace gases throughout the cloud volume.

4. Conclusions

This study examines factors governing NO_3^- concentrations in eastern Pacific Ocean marine clouds with field measurements. The main findings include the following:

(i) The average NO_3^- air-equivalent concentrations in cloud water samples categorized as having been influenced by ship exhaust (2.5 μg m^{-3}), strong marine emissions (2.5 μg m^{-3}) and fires (2.0 μg m^{-3}) were more than twice that in the background cloud water (0.9 μg m^{-3}). Interrelationships between NO_3^-, Na^+ and V show that dissolution of HNO_3 in cloud drops and nucleation scavenging of NO_3^--containing particles are both important sources of this species in cloud water.

(ii) Particulate NO_3^- in the study region was preferentially found in particles with diameters between 1.0 and 5.6 μm, similar to Na, Cl^- and Si, suggesting that drop activation of crustal particles and sea salt could be an important source of NO_3^- in cloud water. Nucleation scavenging of chloride depleted sea-salt is a source of cloud water NO_3^-, with the lowest Cl^-:Na^+ ratio (1.5) observed in ship-influenced samples.

(iii) The average ratio of NO_3^-:SO_4^{2-} was significantly higher in cloud water than below cloud sub-micrometer particles (by a factor of ~11.4 for both campaigns combined), further supporting the notion that NO_3^- enters clouds through the dissolution of HNO_3 and activation of coarse and/or refractory particles not measured by the C-ToF-AMS. The NO_3^-:SO_4^{2-} ratio in cloud droplet residuals was found to be ~80% lower than that in cloud water in both campaigns due mostly to NO_3^- volatilization during drop evaporation. The ratio above cloud tops was consistently higher than below

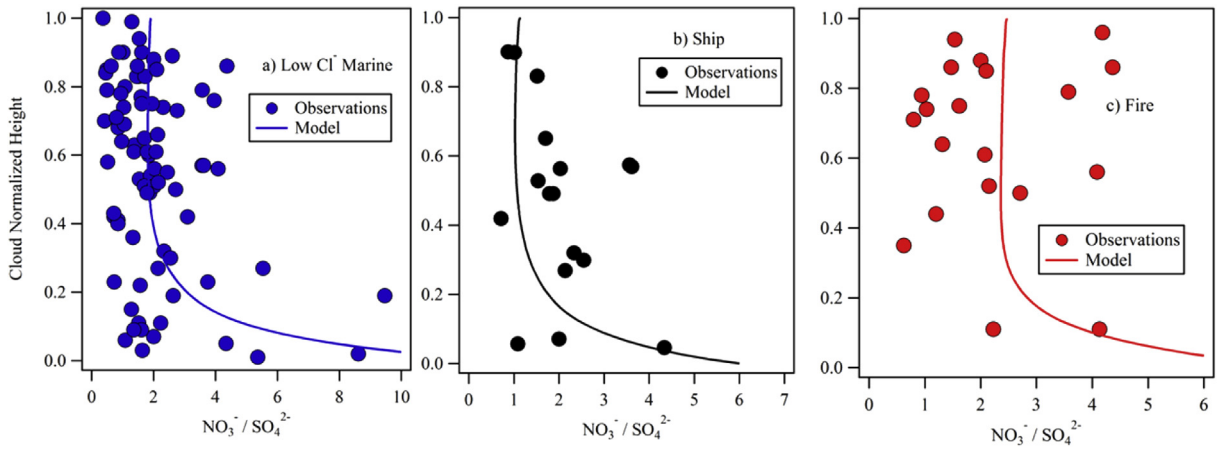

Fig. 6. Vertical profiles of the mass concentration ratio between particulate sulfate and nitrate as a function of normalized cloud height (0 = cloud base, 1 = cloud top). Circular markers denote NiCE observations while curves represent predictions for three modeled cases: (a) "low Cl^- marine", (b) ship and (c) fire. The observed data in the fire case were characterized by entrainment of nitrate and its precursors at cloud top, a process not explicitly included in the model. Initial conditions for parcel model simulations are summarized in Table S3.

clouds (4.3 times higher for both campaigns) due to stronger SO_4^{2-} sources below cloud (e.g., shipping and dimethylsulfide) and elevated NO_3^- above cloud from biomass burning.

(iv) During periods when biomass burning plumes resided above clouds, instability in the entrainment interface layer caused 16 of 29 cloud water samples to exhibit higher NO_3^-, with air-equivalent concentrations reaching up to 9.0 μg m^{-3}.

(v) In the study region, the NO_3^-:SO_4^{2-} mass ratio quickly decreases with cloud height due to the more in-cloud sulfate formation as compared to HNO_3 uptake. In more turbulent clouds, as encountered during biomass burning events, vertical trends in the NO_3^-:SO_4^{2-} ratio cannot be predicted due to cloud top entrainment and the model limitation that cloud depth is equated with processing time scales.

Acknowledgments

This work was funded by Office of Naval Research grants N00014-11-1-0783, N00014-10-1-0200, and N00014-10-1-0811, and National Science Foundation grant AGS-1008848. We acknowledge Dean Hegg for providing the cloud water collector. Barbara Ervens acknowledges support from NOAA's Climate Goal.

Appendix A. Supplementary data

Supplementary data related to this article can be found at http://dx.doi.org/10.1016/j.atmosenv.2014.08.019.

References

Bauer, S.E., Koch, D., Unger, N., Metzger, S.M., Shindell, D.T., Streets, D.G., 2007. Nitrate aerosols today and in 2030: a global simulation including aerosols and tropospheric ozone. Atmos. Chem. Phys. 7, 5043–5059.

Benedict, K.B., Lee, T., Collett, J.L., 2012. Cloud water composition over the southeastern pacific ocean during the VOCALS regional experiment. Atmos. Environ. 46, 104–114. http://dx.doi.org/10.1016/j.atmosenv.2011.10.029.

Borys, R.D., Lowenthal, D.H., Wetzel, M.A., Herrera, F., Gonzalez, A., Harris, J., 1998. Chemical and microphysical properties of marine stratiform cloud in the North Atlantic. J. Geophys. Res. 103 (D17), 22073–22085.

Cautenet, S., Lefeivre, B., 1994. Contrasting behavior of gas and aerosol scavenging in convective rain – a numerical and experimental-study in the African equatorial forest. J. Geophys. Res. 99 (D6), 13013–13024.

Clements, C.B., Zhong, S.Y., Bian, X.D., Heilman, W.E., Byun, D.W., 2008. First observations of turbulence generated by grass fires. J. Geophys. Res. 113, D22,. http://dx.doi.org/10.1029/2008JD010014.

Coggon, M.M., Sorooshian, A., Wang, Z., Metcalf, A.R., Frossard, A.A., Lin, J.J., Craven, J.S., Nenes, A., Jonsson, H.H., Russell, L.M., Flagan, R.C., Seinfeld, J.H., 2012. Ship impacts on the marine atmosphere: insights into the contribution of shipping emissions to the properties of marine aerosol and clouds. Atmos. Chem. Phys. 12, 8439–8458. http://dx.doi.org/10.5194/acp-12-8439-2012.

Coggon, M.M., Sorooshian, A., Wang, Z., Craven, J.S., Metcalf, A.R., Lin, J.J., Nenes, A., Jonsson, H.H., Flagan, R.C., Seinfeld, J.H., 2014. Observations of continental biogenic impacts on marine aerosol and clouds off the coast of California. J. Geophys. Res. 119 http://dx.doi.org/10.1002/2013JD021228.

Drewnick, F., Hings, S.S., DeCarlo, P., Jayne, J.T., Gonin, M., Fuhrer, K., Weimer, S., Jimenez, J.L., Demerjian, K.L., Borrmann, S., Worsnop, D.R., 2005. A new time-of-flight aerosol mass spectrometer (TOF-AMS) – instrument description and first field deployment. Aerosol Sci. Tech. 39, 637–658. http://dx.doi.org/10.1080/02786820500182040.

Drewnick, F., Schneider, J., Hings, S.S., Hock, N., Noone, K., Targino, A., Weimer, S., Borrmann, S., 2007. Measurement of ambient, interstitial, and residual aerosol particles on a mountaintop site in central Sweden using an aerosol mass spectrometer and a CVI. J. Atmos. Chem. 56, 1–20. http://dx.doi.org/10.1007/s10874-006-9036-8.

Ervens, B., Feingold, G., Frost, G.J., Kreidenweis, S.M., 2004. A modeling study of aqueous production of dicarboxylic acids: 1. Chemical pathways and speciated organic mass production. J. Geophys. Res. 109, D15205,. http://dx.doi.org/10.1029/2003JD004387.

Fujitani, Y., Hasegawa, S., Fushimi, A., Kondo, Y., Tanabe, K., Kobayashi, S., Kobayashi, T., 2006. Collection characteristics of low-pressure impactors with various impaction substrate materials. Atmos. Environ. 40, 3221–3229.

Furutani, H., Jung, J., Miura, K., Takami, A., Kato, S., Kajii, Y., Uematsu, M., 2011. Single-particle chemical characterization and source apportionment of iron-containing atmospheric aerosols in Asian outflow. J. Geophys. Res. 116, D18204,. http://dx.doi.org/10.1029/2011JD015867.

Gerber, H., Arends, B.G., Ackerman, A.S., 1994. New microphysics sensor for aircraft use. Atmos. Res. 31, 235–252.

Haman, K.E., Malinowski, S.P., Kurowski, M.J., Gerber, H., Brenguier, J.L., 2007. Small scale mixing processes at the top of a marine stratocumulus – a case study. Q. J. Roy. Meteorol. Soc. 133, 213–226.

Hayden, K.L., Macdonald, A.M., Gong, W., Toom-Sauntry, D., Anlauf, K.G., Leithead, A., Li, S.-M., Leaitch, W.R., Noone, K., 2008. Cloud processing of nitrate. J. Geophys. Res. 113, D18201. http://dx.doi.org/10.1029/2007JD009732.

Hays, M.D., Geron, C.D., Linna, K.J., Smith, N.D., Schauer, J.J., 2002. Speciation of gas-phase and fine particle emissions from burning of foliar fuels. Environ. Sci. Technol. 36, 2281–2295.

Hegg, D.A., Hobbs, P.V., 1986. Studies of the Mechanisms and Rate with Which Nitrogen Species Are Incorporated into Cloud Water and Precipitation. Second Annual Report on Project CAPA-21–80 to the Coordinationg Research Council.

Hegg, D.A., Covert, D.S., Jonsson, H., Covert, P.A., 2005. Determination of the transmission efficiency of an aircraft aerosol inlet. Aerosol Sci. Tech. 39, 966–971. http://dx.doi.org/10.1080/02786820500377814.

Henning, S., Dieckmann, K., Ignatius, K., Schäfer, M., Zedler, P., Harris, E., Sinha, B., van Pinxteren, D., Mertes, S., Birmili, W., Merkel, M., Wu, Z., Wiedensohler, A., Wex, H., Herrmann, H., Stratmann, F., 2014. Influence of cloud processing on CCN activation behaviour in the Thuringian Forest, Germany during HCCT-2010. Atmos. Chem. Phys. Discuss. 14, 1617–1645. http://dx.doi.org/10.5194/acpd-14-1617-2014.

Kavouras, I.G., Nikolich, G., Etyemezian, V., DuBois, D.W., King, J., Shafer, D., 2012. In situ observations of soil minerals and organic matter in the early phases of prescribed fires. J. Geophys. Res. 117, D12. http://dx.doi.org/10.1029/2011JD017420.

Liao, H., Chen, W.T., Seinfeld, J.H., 2006. Role of climate change in global predictions of future tropospheric ozone and aerosols. J. Geophys. Res. 111, D12304. http://dx.doi.org/10.1029/2005JD006852.

Makkonen, R., Romakkaniemi, S., Kokkola, H., Stier, P., Raisanen, P., Rast, S., Feichter, J., Kulmala, M., Laaksonen, A., 2012. Brightening of the global cloud field by nitric acid and the associated radiative forcing. Atmos. Chem. Phys. 12, 7625–7633.

Marjamaki, M., Keskinen, J., 2004. Effect of impaction plate roughness and porosity on collection efficiency. J. Aerosol Sci. 35 (3), 301–308.

Marple, V.A., Rubow, K.L., Behm, S.M., 1991. A microorifice uniform deposit impactor (MOUDI) – description, calibration and use. Aerosol Sci. Tech. 14, 434–446.

Ruellan, S., Cachier, H., Gaudichet, A., Masclet, P., Lacaux, J.P., 1999. Airborne aerosols over central Africa during the experiment for regional sources and sinks of oxidants (EXPRESSO). J. Geophys. Res. 104, 30673–30690.

Russell, L.M., Sorooshian, A., Seinfeld, J.H., Albrecht, B.A., Nenes, A., Ahlm, L., Chen, Y.C., Coggon, M., Craven, J.S., Flagan, R.C., Frossard, A.A., Jonsson, H., Jung, E., Lin, J.J., Metcalf, A.R., Modini, R., Mülmenstädt, J., Roberts, G.C., Shingler, T., Song, S., Wang, Z., Wonaschütz, A., 2013. Eastern Pacific emitted aerosol cloud experiment (E-PEACE). Bull. Am. Met. Soc. 94, 709–729. http://dx.doi.org/10.1175/BAMS-D-12-00015.1.

Seinfeld, J.H., Pandis, S.N., 2006. Atmospheric Chemistry and Physics, Second ed. Wiley-Interscience, New York.

Shingler, T., Dey, S., Sorooshian, A., Brechtel, F.J., Wang, Z., Metcalf, A., Coggon, M., Mulmenstadt, J., Russell, L.M., Jonsson, H.H., Seinfeld, J.H., 2012. Characterization and airborne deployment of a new counter flow virtual impactor inlet. Atmos. Meas. Tech. 5, 1259–1269. http://dx.doi.org/10.5194/amt-5-1259-2012.

Sorooshian, A., Wang, Z., Coggon, M., Jonsson, H., Ervens, B., 2013. Observations of sharp oxalate reductions in stratocumulus clouds at variable altitudes: organic acid and metal measurements during the 2011 E-PEACE campaign. Environ. Sci. Tech. 47, 7747–7756. http://dx.doi.org/10.1021/es4012383.

Straub, D.J., Lee, T., Collett, J.L., 2007. Chemical composition of marine stratocumulus clouds over the eastern Pacific ocean. J. Geophys. Res. 112, D04307. http://dx.doi.org/10.1029./2006JD007439.

Stull, R.B., 2003. An Introduction to Boundary Layer Meteorology. Kluwer Academic Publishers, The Netherlands.

Wang, Z., Sorooshian, A., Prabhakar, G., Coggon, M.M., Jonsson, H.H., 2014. Impact of emissions from shipping, land and the ocean on stratocumulus cloud water elemental composition during the 2011 E-PEACE field campaign. Atmos. Environ. 89, 570–580. http://dx.doi.org/10.1016/j.atmosenv.2014.01.020.

Wonaschütz, A., Hersey, S.P., Sorooshian, A., Craven, J.S., Metcalf, A.R., Flagan, R.C., Seinfeld, J.H., 2011. Impact of a large wildfire on water-soluble organic aerosol in a major urban area: the 2009 station fire in Los Angeles County. Atmos. Chem. Phys. 11, 8257–8270.

Xue, H., Feingold, G., 2004. A modeling study of the effect of nitric acid on cloud properties. J. Geophys. Res. 109, D18204,. http://dx.doi.org/10.1029/2004JD004750.